OPEN ACCESS

Original research

Combining ferroptosis induction with MDSC blockade renders primary tumours and metastases in liver sensitive to immune checkpoint blockade

Claire Conche,[1,2] Fabian Finkelmeier ,[1,2,3] Marina Pešić,[1,2] Adele M Nicolas,[1,2] Tim W Böttger,[1,2] Kilian B Kennel,[1,2] Dominic Denk,[1,2,3] Fatih Ceteci,[1,2] Kathleen Mohs,[1,2] Esther Engel,[1,2] Özge Canli,[1] Yasamin Dabiri,[1,2] Kai-Henrik Peiffer ,[3] Stefan Zeuzem,[3] Gabriela Salinas,[4] Thomas Longerich ,[5] Huan Yang,[6] Florian R Greten [1,2,7]

► Additional supplemental material is published online only. To view, please visit the journal online (http://dx.doi.org/10.1136/gutjnl-2022-327909).

For numbered affiliations see end of article.

Correspondence to
Professor Florian R Greten, Institute for Tumor Biology and Experimental Therapy, Frankfurt/Main 60596, Germany; greten@gsh.uni-frankfurt.de

CC and FF contributed equally.

CC and FF are joint first authors.

Received 21 May 2022
Accepted 7 January 2023
Published Online First 27 January 2023

► http://dx.doi.org/10.1136/gutjnl-2023-329472

To cite: Conche C, Finkelmeier F, Pešić M, *et al*. *Gut* 2023;**72**:1774–1782.

ABSTRACT

Objective Investigating the effect of ferroptosis in the tumour microenvironment to identify combinatory therapy for liver cancer treatment.

Design Glutathione peroxidase 4 (GPx4), which is considered the master regulator of ferroptosis, was genetically altered in murine models for hepatocellular carcinoma (HCC) and colorectal cancer (CRC) to analyse the effect of ferroptosis on tumour cells and the immune tumour microenvironment. The findings served as foundation for the identification of additional targets for combine therapy with ferroptotic inducer in the treatment of HCC and liver metastasis.

Results Surprisingly, hepatocyte-restricted GPx4 loss does not suppress hepatocellular tumourigenesis. Instead, GPx4-associated ferroptotic hepatocyte death causes a tumour suppressive immune response characterised by a CXCL10-dependent infiltration of cytotoxic $CD8^+$ T cells that is counterbalanced by PD-L1 upregulation on tumour cells as well as by a marked HMGB1-mediated myeloid derived suppressor cell (MDSC) infiltration. Blocking PD-1 or HMGB1 unleashes T cell activation and prolongs survival of mice with *Gpx4*-deficient liver tumours. A triple combination of the ferroptosis inducing natural compound withaferin A, the CXCR2 inhibitor SB225002 and α-PD-1 greatly improves survival of wild-type mice with liver tumours. In contrast, the same combination does not affect tumour growth of subcutaneously grown CRC organoids, while it decreases their metastatic growth in liver.

Conclusion Our data highlight a context-specific ferroptosis-induced immune response that could be therapeutically exploited for the treatment of primary liver tumours and liver metastases.

WHAT IS ALREADY KNOWN ON THIS TOPIC

⇒ Glutathione peroxidase 4 has been suggested to confer tumour suppressive functions in a cell autonomous manner.
⇒ $CD8^+$ T cells can induce ferroptosis in tumour cells.

WHAT THIS STUDY ADDS

⇒ In hepatocellular carcinoma (HCC), ferroptosis does not provide a cell autonomous tumour suppressor function, but rather triggers an adaptive immune response placing ferroptosis upstream of $CD8^+$ T cells.
⇒ T cell infiltration by cCAS/STING-dependent CXCL10 secretion is associated with IFNγ secretion by $CD8^+$ T cells, ultimately resulting in PD-L1 upregulation on tumour cells.
⇒ On the contrary, ferroptosis triggers tumour infiltration of myeloid derived suppressor cells (MDSCs) via HMGB1 in HCC but not in colorectal cancer (CRC).
⇒ Ferroptosis is as potent anticancer target for the treatment of HCC and CRC liver metastasis in combination with immune checkpoint and MDSC blockade while primary CRC is resistant to this combinatorial treatment.

HOW THIS STUDY MIGHT AFFECT RESEARCH, PRACTICE OR POLICY

⇒ Provide a novel therapeutic option for the treatment HCC and CRC liver metastasis.
⇒ The withaferin A (WFA), α-PD-1 and SB225002 combinatory treatment could potentially extend to liver metastases from other tumour types considering that its efficacy on liver metastasis is independent on the primary tumour response and that ferroptosis is a non-targeted antitumour approach.

INTRODUCTION

Ferroptosis is a non-apoptotic iron-dependent type of cell death that depends on the accumulation of lipid peroxides that cause disruption of cell membranes.[1 2] Ferroptosis differs from other types of cell death by cellular morphology and the responsible signalling pathways as it cannot be rescued by caspase-associated, receptor-associated adaptor kinase (RIP) and tumour necrosis factor α (TNFα) inhibition while it is sensitive to reducing and iron chelating agents.[3] Although the terminal executive molecular mechanisms of ferroptosis are yet to be clearly identified the initials signals regulating lipid peroxidation are well documented. Physiologically, ferroptosis is prevented by the

selenoenzyme glutathione peroxidase 4 (GPx4) which comprises an important constituent of the cellular antioxidant network.[4] GPx4 activity depends on glutathione whose concentration relies on cysteine import by the System Xc^-. Not surprisingly lipoxygenase (ALOX), polyunsaturated fatty acids, which are sensitive to lipid peroxidation acetyl-CoA enzymes have been shown to be involved in ferroptosis.[5]

Cancer cells tend to be more sensitive to ferroptosis which might be correlated to their oncogenic profiles.[5] Indeed, tumour suppressors p53 and BAP1 regulate the expression of SCL7A11 and thereby the sensitivity of tumour cells to ferroptosis.[6 7] Additionally, p53 has been shown to modulate ferroptosis through alternative pathways including Alox and P21.[8] Retinoblastoma proteins have been reported to correlate with the ferroptotic resistance in hepatocellular carcinoma (HCC).[9] The role of Ras in the regulation of ferroptosis has to be elucidated and might be context dependent with reports of RAS either promoting or limiting ROS and ferroptosis.[10] Ferroptosis can be triggered either by increasing the cellular iron load and ROS generation or by inhibiting the antioxidant machinery. Among ferroptosis targeting pharmacological agents available, Erastin, inhibitor of System Xc^- and RSL3 and withaferin A (WFA) all of which inhibit GPx4 are potent ferroptosis inducers.[11 12] Importantly, sorafenib, which has been used for a long time as a first-line therapy for advanced HCC induces ferroptosis[13] while ferroptosis in non-viral and non-tumour liver diseases tends to aggravate the pathology.[14] Paradox effects of ferroptosis were also reported for pancreatic cancer.[15] Interestingly, there is also a link between ferroptosis and immune cell activation. IFNγ and arachidonic acid releasing $CD8^+$ T cells trigger an ACSL4-dependent ferroptosis.[16 17] Moreover, ferroptosis associated 8-OHdG activates the STING pathway and triggers macrophage infiltration and M2-polarisation thereby promoting pancreatic tumourigenesis.[18 19] Early ferroptotic but not late ferroptotic cells can trigger T cell mediated antitumuor vaccination in a fibrosarcoma murine model[20] raising the possibility that a ferroptosis-dependent cytotoxic antitumourigenic adaptive immune response may be context dependent.

Here, we describe the contribution of hepatocyte ferroptosis to $CD8^+$ T cell activation in a model of primary HCC and metastatic colon cancer and identify the complex interaction between cancer, myeloid and T cells within the liver tumour microenvironment that could offer a new therapeutic approach for the treatment of HCC and liver metastases.

RESULTS

Hepatocyte restricted GPX4 deletion induces ferroptosis and inflammation

To examine GPx4 function in liver, we crossed floxed *Gpx4* mice ($Gpx4^{F/F}$) to albumin-Cre expressing mice to generate $Gpx4^{\Delta/\Delta hep}$ mice. In vivo, *Gpx4* deletion is usually compensated by the high amount of vitamin E typically present in regular chow.[7 21–23] Accordingly, while $Gpx4^{F/F}$ mice were healthy, $Gpx4^{\Delta/\Delta hep}$ mice succumbed to liver failure within 21 days when placed on a vitamin E-depleted diet ($diet^{\Delta vitE}$), which was not observed when mice were kept on a regular chow (online supplemental figure 1A). Gpx4-dependent liver damage was characterised by distinct zonal necrosis accompanied by sinusoidal congestion, haemorrhage and signs of immune cell infiltration (online supplemental figure 1B). In line with ferroptosis induction in vivo, hepatocytes from $Gpx4^{\Delta/\Delta hep}$ mice on $diet^{\Delta vitE}$ were TUNEL positive while caspase-3 negative with increased expression of lipids peroxidation markers MDA and 4-HNE as well of the newly identify ferroptotic marker CD71[24] (online supplemental figure 1B). Induction of ferroptosis was further confirmed in primary $Gpx4^{\Delta/\Delta hep}$ hepatocytes ex vivo that could only survive in the presence of ferroptosis inhibitors (online supplemental figure 1C). RNAseq analysis and *GOterm* pathway analysis of livers from $Gpx4^{F/F}$ and $Gpx4^{\Delta/\Delta hep}$ mice revealed a significant enrichment of genes connected to inflammatory and immune response pathways (online supplemental figure 1D,E) confirming that hepatocyte-specific Gpx4 deletion causes ferroptosis in vitro as well as in vivo leading to acute liver failure and inflammation.

Ferroptosis does not suppress HCC development

Given that many of the gene products upregulated in ferroptotic livers are known to promote tumour development,[25] we reasoned that during tumourigenesis, ferroptosis may counteract the previously suggested cell autonomous tumour suppression[6 7] by creating a proinflammatory, protumourigenic microenvironment. Thus, to examine the consequences of *Gpx4* loss during liver tumourigenesis, we took advantage of a transposon-based mouse model of liver cancer,[21 26] that is achieved by hydrodynamic tail vein injection (HTVI) of a construct encoding for two oncogenes, $Nras^{G12V}$ and *myr*AKT, together with a transposase encoding plasmid (figure 1A). Nras immunostainings confirmed similar efficiency in transposon delivery after 7 days in both genotypes (figure 1B) and led to multifocal HCC 25 days after HTVI that imposed as highly differentiated hepatocellular tumours with trabecular growth pattern, prominent nucleoli and variable fatty changes and ballooning (figure 1C). In some parts regressive and inflammatory changes could be observed. Moreover, Pearl's Prussian blue staining did not indicate any evidence for enhanced iron deposition in the livers of $Gpx4^{F/F}$ or $Gpx4^{\Delta/\Delta hep}$ mice after HTVI (online supplemental figure 2F). Liver tumours in $Gpx4^{\Delta/\Delta hep}$ mice were characterised by a marked increase in the number of TUNEL-positive cells while the number of apoptotic cells determined by cleaved caspase3 did not differ (figure 1D). Additionally, tumours form $Gpx4^{\Delta/\Delta hep}$ mice showed a significant increase of lipid peroxidation, CD71 expression as well as p-H2AX expression which was associated with elevated levels of oxidative DNA damage marker 8-OHdG (figure 1D), supporting the notion that *Gpx4*-deficient tumour cells died from non-apoptotic, lipid peroxidation induced ferroptosis. Remarkably, tumour load, tumour cell proliferation and survival rates of HCC tumour-bearing mice were comparable between $Gpx4^{F/F}$ controls and $Gpx4^{\Delta/\Delta hep}$ mice (figure 1E,F). Thus, induction of ferroptosis in HCC was not sufficient to confer a significant tumour suppression.

Ferroptosis induces $CD8^+$ T cell activation that is counteracted by PD-L1 upregulation on tumour cells

Considering the ferroptosis-associated inflammatory response during liver failure (online supplemental figure 1D,E), we examined gene expression profiles on day 25 of the transposon-induced HCC model and found a similar upregulation of several chemokines and cytokines (figure 2A) indicating that tumour-associated hepatocyte ferroptosis triggered an immune reaction. Immunofluorescence revealed an increased number of $CD3^+$ and $CD8^+$ T cells in $Gpx4^{\Delta/\Delta hep}$ tumours which, however, was accompanied by a marked upregulation of PD-L1 in tumours (figure 2B). PD-L1 upregulation on tumour cells did not correlate with an overall increased T cell exhaustion in $Gpx4^{\Delta/\Delta hep}$ tumours based on a comparable expression of activation and exhaustion markers comparing $CD8^+$ T cells from $Gpx4^{\Delta/\Delta hep}$ and $Gpx4^{F/F}$ tumours

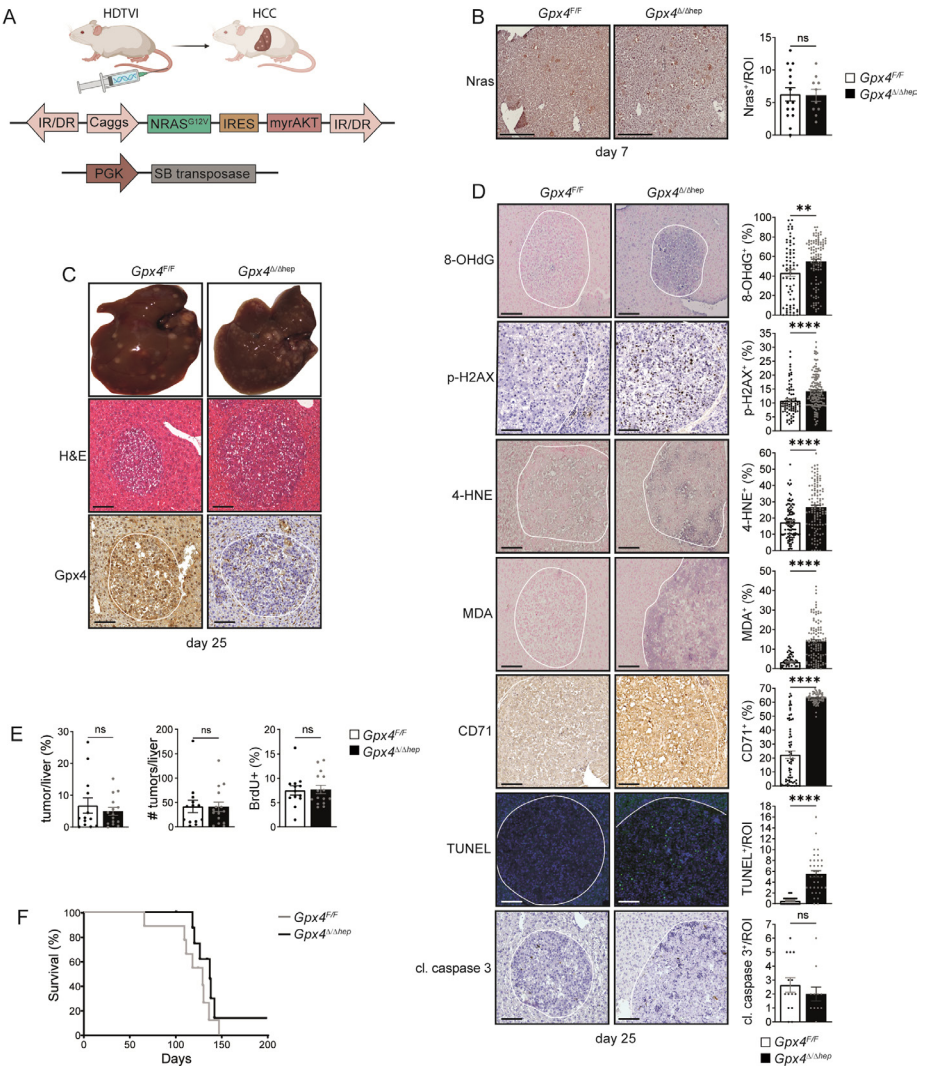

Figure 1 Ferroptotic induction in a murine model of HCC is not sufficient to limit tumour growth. (A) Scheme of HCC murine model with HTVI of oncogenic Nrsas^{G12V} and myristoylated-AKT together with sleeping beauty (SB). (B) Nras immunohistochemical analysis in livers of *Gpx4*$^{F/F}$ and *Gpx4*$^{\Delta/\Delta hep}$ mice 7 days after HTVI (n≥10). (C) Representative images of multifocal HCC and H&E and Gpx4-IHC staining of livers of *Gpx4*$^{F/F}$ and *Gpx4*$^{\Delta/\Delta hep}$ mice 25 days after HTVI. (D) Immunohistochemical analysis of 8-OHdG$^+$ (n≥=73), p-H2AX$^+$ (n≥80), 4-HNE$^+$ (n≥99), MDA$^+$ (n≥59), CD71$^+$ (n≥69), cleaved-caspase 3$^+$ (n≥11) and TUNEL$^+$ (n≥=30) cells in liver tumours of *Gpx4*$^{F/F}$ and *Gpx4*$^{\Delta/\Delta hep}$ mice. (E) Quantification of tumour area percentage to the liver and number of tumours per liver from H&E-stained serial sections. Immunohistochemical analysis of BrdU incorporation in tumours (n≥13). (F) Survival of *Gpx4*$^{F/F}$ and *Gpx4*$^{\Delta/\Delta hep}$ mice after HTVI (n=9), p=0176 by log-rank (Mantel-Cox) test. (A–E) Scale bars=100 µm. Data are mean±SEM, n.s. not significant, **p≤0.01, ****p≤0.0001 by t-test. HCC, hepatocellular carcinoma; HTVI, hydrodynamic tail vein injection; IR/DR, inverted repeats and direct repeats; IRES, internal ribosome entry site.

(online supplemental figure 2A). Instead, CD8$^+$ T cells isolated from *Gpx4*$^{\Delta/\Delta hep}$ ferroptotic tumours had the ability to secrete more IFNγ than CD8$^+$ T cells from control tumours, demonstrating that ferroptosis increased functional activation of the CD8$^+$ T cells (figure 2C). Antibody-mediated CD8$^+$ T cell depletion confirmed that PD-L1 upregulation in tumours was a consequence of enhanced CD8$^+$ T cell infiltration (figure 2D). Next, we aimed to elucidate the link between hepatocyte ferroptosis and CD8$^+$ T cell infiltration. Among the chemokines upregulated in *Gpx4*$^{\Delta/\Delta hep}$ tumours (figure 2A), CXCL10 represents a potent T cell chemoattractant. Freshly isolated primary ferroptotic *Gpx4*$^{\Delta/\Delta hep}$ hepatocytes secreted increased amounts of CXCL10 (figure 2E) confirming that CXCL10 secretion was a direct consequence of ferroptosis. Importantly, deletion of CXCL10 receptor *Cxcr3* prevented CD8$^+$ T cell infiltration into *Gpx4*$^{\Delta/\Delta hep}$ tumours as well as the subsequent CD8$^+$ T cell dependent PD-L1 upregulation (figure 2F,G) underlining the crucial role of hepatocyte-released CXCL10 as a consequence of ferroptosis in driving CD8$^+$ T cell infiltration in *Gpx4*$^{\Delta/\Delta hep}$ tumours. Recently, DNA damage has been associated with induction of CXCL10 as well as other proinflammatory genes,[27] while in pancreatic cancer ferroptosis-induced 8-OHdG formation led to STING activation.[18] Therefore, we examined whether STING blockade would impact CXCL10 secretion. Indeed, CXCL10 release by *Gpx4*$^{\Delta/\Delta hep}$ ferroptotic hepatocytes was sensitive to cGAS/STING inhibitors (figure 2H), consistent with STING dependent macrophage infiltration in pancreatic cancer.[18] Furthermore, we hypothesised that PD-L1 upregulation impaired the ferroptosis-induced T cell antitumour response, which could benefit from α-PD-1 therapy. Consequently, we subjected HCC-bearing mice to immune checkpoint

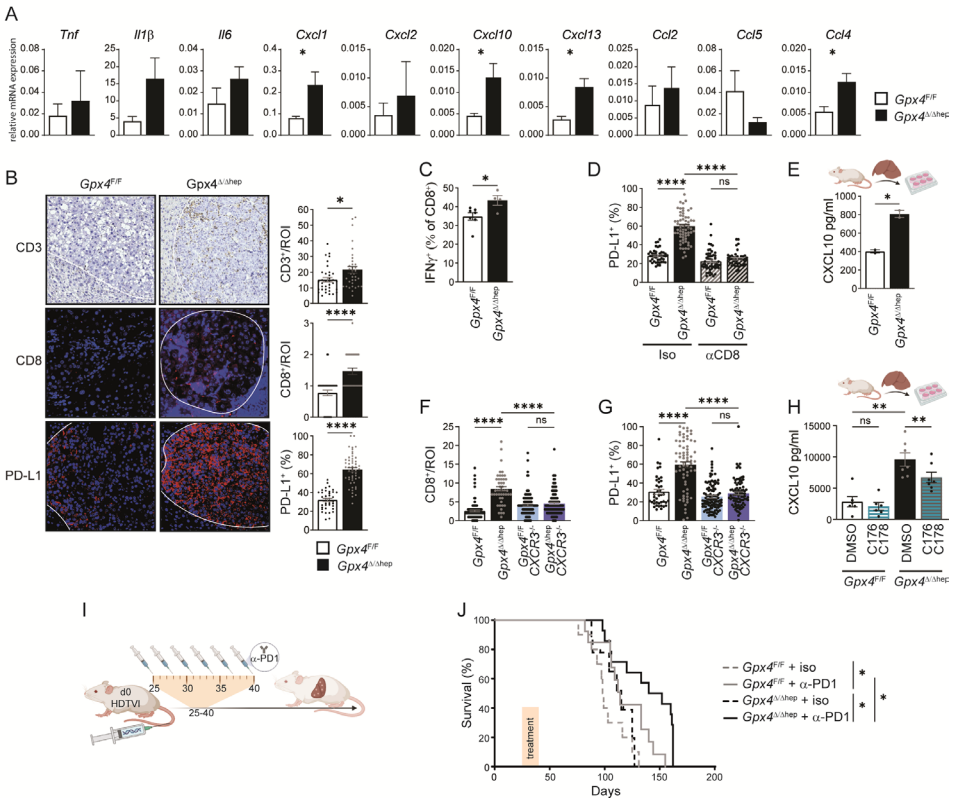

Figure 2 Ferroptosis in HCC induces immune reaction with T cell activation dampened by PD-L1 upregulation. (A) Gene expression quantification by quantitative RT-PCR in tumours from *Gpx4*$^{F/F}$ and *Gpx4*$^{\Delta/\Delta hep}$ mice 25 days after HTVI (n=5). (B) Immunohistochemical analysis of CD3$^+$ (n=35), CD8 (n≥36), PD-L1$^+$ (n=38) cells in HCC tumours of *Gpx4*$^{F/F}$ and *Gpx4*$^{\Delta/\Delta hep}$ mice after HTVI. Scale bars=100 µm. (C) Flow cytometry analysis of IFNγ expression in CD8 T cells from liver of *Gpx4*$^{F/F}$ and *Gpx4*$^{\Delta/\Delta hep}$ tumour bearing mice after PMA/Ionomycin stimulation (n≥4). (D) Immunofluorescence quantification of PD-L1 expression in HCC tumours from *Gpx4*$^{F/F}$ *and Gpx4*$^{\Delta/\Delta hep}$ mice treated with depleting α-CD8 or Rat IgG2b, κ antibodies (n≥42). (E) CXCL10 release by primary hepatocytes from *Gpx4*$^{F/F}$ and *Gpx4*$^{\Delta/\Delta hep}$ mice ex vivo for 4 hours (n=2). (F, G) Immunofluorescence quantification of CD8$^+$ T cells infiltration (F) and PD-L1 expression (G) in HCC tumours from *Gpx4*$^{F/F}$, *Gpx4*$^{\Delta/\Delta hep}$, *Gpx4*$^{F/F}$*CXCR3*$^{-/-}$, *Gpx4*$^{\Delta/\Delta hep}$*CXCR3*$^{-/-}$ mice (n≥40). (H) CXCL10 secretion by *Gpx4*$^{F/F}$ and *Gpx4*$^{\Delta/\Delta hep}$ primary hepatocytes ex vivo treated with 10 µM of C176 and C178 or DMSO for 4 hour (n≥6). (I) Treatment scheme for i.p. injections, of α-PD-1 or isotype (Rat IgG2a,κ). (J) Survival of *Gpx4*$^{F/F}$+ isotype (Rat IgG2a,κ) (n=10), *Gpx4*$^{F/F}$ + α-PD-1 (n=13), *Gpx4*$^{\Delta/\Delta hep}$ + isotype (Rat IgG2a,κ) (n=9) and *Gpx4*$^{\Delta/\Delta hep}$ +α-PD-1 (n=14) mice with HCC tumours. (A–H) Data are mean±SEM, n.s not significant *p≤0.05, **p≤0.01, ****p≤0.0001 by t-test (A–C, E) or one-way ANOVA with Šídák's multiple comparisons test (D, F–H) of the indicated pairs or by log-rank (Mantel-Cox) test (J). ANOVA, analysis of variance; HTVI, hydrodynamic tail vein injection; PMA, phorbol myristate acetate.

blockade and injected α−PD-1 every 3 days for 16 days starting at day 25 (figure 2I) when we detected immune cell infiltration (figure 2A.B). Even though we applied only one cycle of six injections, α-PD-1 treated *Gpx4*$^{\Delta/\Delta hep}$ mice had a significantly increased survival advantage compared with *Gpx4*$^{\Delta/\Delta hep}$ isotype treated mice or to WT mice treated with α-PD-1 (figure 2J). Thus, ferroptosis triggered a tumour suppressive CD8$^+$ T cell response, which was counteracted by a concomitant PD-L1 upregulation that could be unleashed by α−PD-1 treatment.

Ferroptosis induces immunosuppression by stimulating myeloid derived suppressor cell recruitment

In addition to the pronounced CD8$^+$ T cell infiltration, we also observed enhanced F4/80$^+$ and Gr-1$^+$ myeloid cell infiltration into *Gpx4*$^{\Delta/\Delta hep}$ tumours (figure 3A), comprising potentially myeloid derived suppressor cells (MDSCs) and tumour-associated macrophages (TAMs). Flow cytometric analysis was performed to further characterise the myeloid compartment. We found that neither recruitment of TAMs nor recruitment and activation of dendritic cells (DC) was affected by ferroptosis in *Gpx4*$^{\Delta/\Delta hep}$ tumours (online supplemental figure 3A,B), while M-MDSC and PMN-MDSC infiltration was significantly increased in *Gpx4*$^{\Delta/\Delta hep}$ tumours (figure 3B). The immunosuppressive activity of tumour infiltrating MDSC on T cell proliferation was confirmed and we noticed that ferroptosis significantly increased PMN-MDSC immunosuppressive activity (figure 3C). Next, we investigated how ferroptosis triggered MDSC infiltration in *Gpx4*$^{\Delta/\Delta hep}$ tumours. HMGB1 is a potent recruiter of MDSCs[28] and we could indeed confirm that primary *Gpx4*$^{\Delta/\Delta hep}$ hepatocytes undergoing ferroptosis released significantly higher levels of HMGB1 than control hepatocytes (figure 3D). To test whether HMGB1 blockade would prevent MDSC infiltration and stimulate anti-tumour immunity in *Gpx4*$^{\Delta/\Delta hep}$ mice, we either induced HCC in *Gpx4*$^{\Delta/\Delta hep}$/*Rage*$^{-/-}$ compound mutant mice or treated tumour-bearing *Gpx4*$^{\Delta/\Delta hep}$ single mutant mice with HMGB1 neutralising antibody for 2 weeks starting on day 25 (figure 3E,F). While α-HMGB1 antibody treatment shifted the median survival from

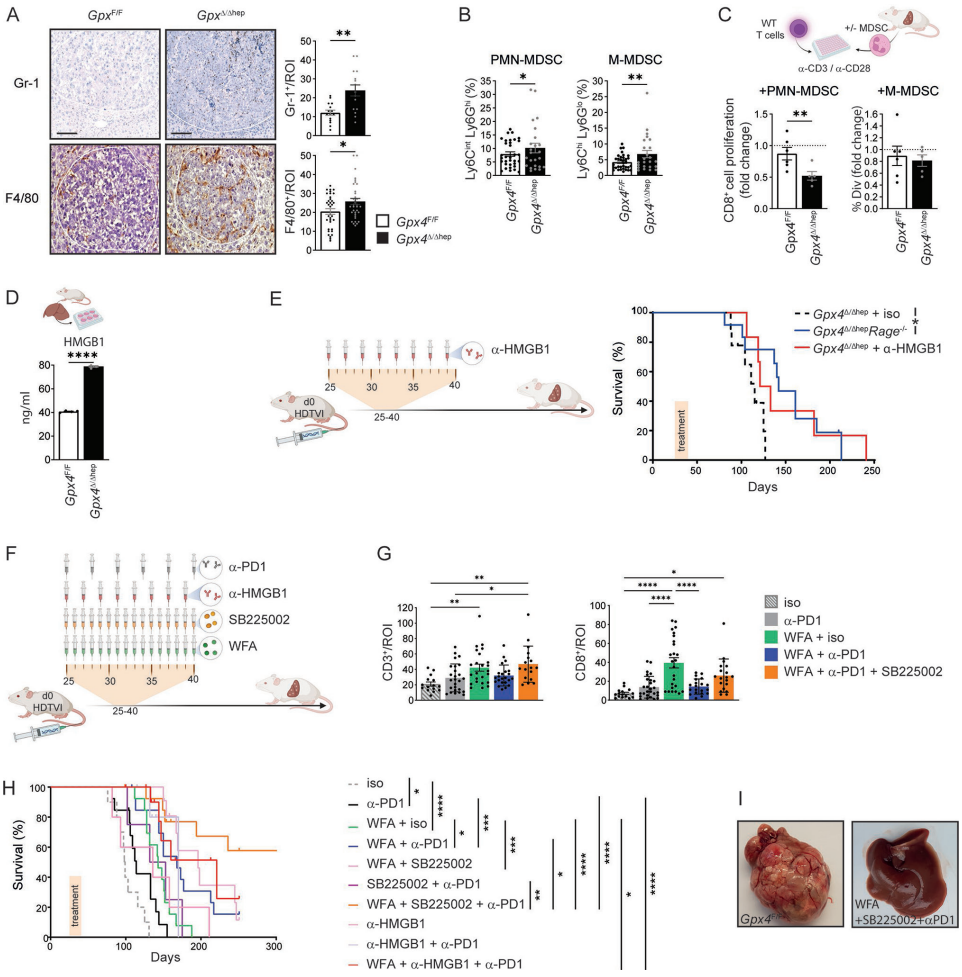

Figure 3 T cell activation and MDSC tumour infiltration induced by ferroptosis serve as targets for combinatory therapy for HCC. (A) Immunohistochemical analysis of Gr-1$^+$ (n=15) and F4/80$^+$ (n=35) cells in *Gpx4*$^{F/F}$ and *Gpx4*$^{\Delta/\Delta hep}$ HCC tumours. scale bars=100 µm. (B) Flow cytometry quantification of the percentages of PMN-MDSC and M-MDSC within the CD45$^+$infiltrates of livers from *Gpx4*$^{F/F}$ and *Gpx4*$^{\Delta/\Delta hep}$ HCC tumour-bearing mice. (n≥22). (C) Immunosuppression of MDSC isolated from livers of *Gpx4*$^{F/F}$ and *Gpx4*$^{\Delta/\Delta hep}$ tumour bearing mice on CD8$^+$ T cell proliferation. Fold change of the percentages of divided CD8$^+$ T cells with MDSC to CD8$^+$ T cells without MDSC (n≥5). (D) HMGB1 release by primary hepatocytes from *Gpx4*$^{F/F}$ and *Gpx4*$^{\Delta/\Delta hep}$ mice ex vivo for 4 hours (n=2). (E) Survival of *Gpx4*$^{\Delta/\Delta hep}$ mice treated with isotype Rat IgG2a,κ (as in 2J, n=9) or α-HMGB1 (n=6) and untreated *Gpx4*$^{\Delta/\Delta hep}$*/Rage*$^{-/-}$ (n=12) mice after HTVI. (F) Treatment scheme with i.p. injections of 250 µg of α-PD-1 or isotype (Rat IgG2a,κ), 50 µg of α-HMGB1, 2.5 mg/kg of WFA or 1 mg/kg of SB225002. (G) Immunohistochemical analysis of CD3$^+$ or CD8$^+$ T cell infiltration in HCC tumours of *Gpx4*$^{F/F}$ and *Gpx4*$^{\Delta/\Delta hep}$ mice>100 days after HTVI (n≥15). (H) Survival of WT mice after HTVI receiving Isotype (Rat IgG2a,κ) (n=10), α-PD-1 (n=13) (as in figure 2), WFA+isotype (Rat IgG2a,κ) (n=13), WFA + α-PD-1(n=14), WFA+SB225002 (n=12), SB225002 + α-PD-1 (n=13), WFA+SB225002 + α-PD-1 (n=14), α-HMGB1 (n=5), α-HMGB1 + α-PD1 (n=6) or WFA + α-HMGB1 + α-PD1 (n=12) treatments. (I) Pictures of livers of untreated *Gpx4*$^{F/F}$ mice at end point and WT mice treated with WFA+SB225002+α-PD-1 >300 days after HTVI. (A–H) Data are mean±SEM, *p≤0.05, **p≤0.01, ***p≤0.001, ****p≤0.0001 by t-test (A–D) one-way ANOVA with Šídák's's multiple comparisons of all groups (G) or by log-rank (Mantel-Cox) test (E, H). ANOVA, analysis of variance; HCC, hepatocellular carcinoma; HTVI, hydrodynamic tail vein injection; MDSC, myeloid derived suppressor cell; WFA, withaferin A.

113 to 127 days (p=0,0816), *Rage* deletion prolonged overall survival of *Gpx4*$^{\Delta/\Delta hep}$ mice significantly (figure 3E), yet in both cases some mice survived more than 200 days highlighting the tumour promoting role of MDSC on ferroptosis induction and supporting the notion that ferroptosis-associated HMGB1 release mediated infiltration of immunosuppressive PMN-MDSCs and M-MDSC counteracted a cytotoxic T cell response.

Considering that both blocking PD-1 or MDSC recruitment prolonged survival of *Gpx4*$^{\Delta/\Delta hep}$ mice with HCC, we wanted to examine whether pharmacological ferroptosis induction while targeting both immunosuppressive pathways, MDSCs and PD-1, could represent a therapeutic option for HCC treatment. To this end we generated liver tumours in WT mice and treated with WFA, a natural anticancer agent shown to induce ferroptosis by lipid peroxidation in vivo.[11] Additionally, mice were treated either with α−PD-1, the α−HMGB1 neutralising antibody or alternatively the CXCR2 inhibitor SB225002, a potent blocker of myeloid cell recruitment.[29] Tumour-bearing mice were treated for only 2 weeks starting on day 25 of the model (figure 3F). Analysis of CD3$^+$ and CD8$^+$ T cell infiltration in hepatic tumours after more than 100 days demonstrated that WFA treatment resulted in a long-lasting T cell infiltration, while blocking PD-1 alone or in combination with other compounds did not enhance T cell infiltration further (figure 3G) underlining the important contribution of ferroptosis for intratumoural T cell infiltration. While single administration of α-PD-1 improved survival by only 14.5 days, WFA monotreatment prolonged median survival by 44.5 days, yet the combination of these two was even more

effective (figure 3H) further supporting the notion that ferroptosis sensitises for checkpoint inhibition. However, when HMGB1 was blocked additionally, 50% of mice survived more than 200 days (online supplemental figure 3D). Treatment with α-HMGB1 significantly improved survival only when combined with WFA and α-PD-1 compared with WFA or α-PD-1 monotherapies (online supplemental figure 3D). However, employing SB225002 to block MDSC infiltration instead of α-HMGB1 along with both WFA and αPD-1 led to better survival rates. Indeed, the triple combination of WFA, α-PD-1 and SB225002 led to survival of 60% of mice for more than 300 days at which time livers were completely tumour free (figure 3H,I). Thus, although given only over a period of 2 weeks, the treatments provided a long-lasting effect in this highly aggressive model. Collectively, these data emphasise the need of targeting MDSCs to achieve the full potential of ferroptosis induction and PD-1 blockade.

Ferroptosis-associated cytotoxic T cell response provides tumour suppression only in liver

To examine whether tumour cell ferroptosis would trigger a comparable anti-tumour immune response also in other tumour entities, we took advantage of recently developed colorectal tumour organoids mutant for *Apc*, *Trp53*, *Tgfbr2*, *K-ras*^{G12D} (APTK) or additionally expressing a myristoylated AKT (APTKA) that can be transplanted into immunocompetent mice.[30 31] Doxycycline inducible shRNAs targeting *Gpx4* or control shRNA were introduced in both APTK and APTKA organoids and subcutaneous (s.c.) tumours were generated. Loss of Gpx4 protein expression and CD71 upregulation as a marker for ferroptosis induction in APTKA and APTK s.c. tumours expressing sh*Gpx4* were confirmed by immunohistochemistry (figure 4A,B and data not shown). Like in the HCC model loss of *Gpx4* alone did not affect tumour growth of s.c. colorectal tumours (figure 4C), yet flow cytometric analysis confirmed enhanced CD4$^+$ and CD8$^+$ T cell infiltration (online supplemental figure 4A) accompanied by increased IFNγ secretion by CD8$^+$ T cells (figure 4D) in *Gpx4*-deficient tumours that were further characterised by a T cell-dependent PD-L1 upregulation (figure 4E). CD8$^+$ T cells did not reveal any significant changes in the expression of CD69, PD-1, TIM3, CTLA-4 or Lag3 (online supplemental figure 4B). Similar to HCC, TAMs were not increased in Gpx4-deficient colorectal tumours, while DC and M-MDSC infiltration was enhanced (figure 4F). However, in contrast to the HCC model, PMN-MDSC infiltration was markedly reduced in the s.c. colorectal organoid-induced tumours (figure 4F). To evaluate whether the triple combination of pharmacological ferroptosis induction, MDSC suppression and checkpoint blockade could be successfully transferred to colorectal tumours, we treated APTKA or APTK tumours starting on day 7 for 2 weeks with WFA, SB225002 and α-PD-1. However, in contrast to HCC treatment the triple combination did not reduce primary colorectal tumour growth (figure 4G,H). To examine whether the lack of treatment response was due to the different tumour entity (colon vs HCC), the different underlying mutational spectrum or because tumours were treated outside the liver, we treated s.c. tumours derived from tumour cells that had been generated by HTVI of Nras^{G12V} and *myr*AKT in *p19*$^{-/-}$ mice.[32] However, the combined administration of WFA, α-PD-1 and SB225002 did not impair growth of these s.c. HCC established outside the liver (figure 4I,J) suggesting that sensitivity to triple therapy was defined by the tumour microenvironment rather than the tumour entity or the genetic profile. To confirm this, we refined a model of liver metastasis[33] and injected 50 000 APTK organoids into the spleen, which led to the development of liver metastases within 5 days at which point we initiated treatment (figure 4K). The individual administration of either SB225002, α-PD-1 or WFA alone did not affect the number of liver metastases (figure 4L). However, as expected, the combination of all three compounds significantly reduced the number of colorectal liver metastasis (figure 4L). Similarly, liver tumours induced by intrasplenic injection of 15 000 Nras^{G12V}/*myr*AKT/*p19*$^{-/-}$ HCC cells (figure 4M) responded well to the combination of SB225002, α−PD-1 and WFA (figure 4N). Collectively, these data highlight the niche specific immune response to ferroptosis and suggest that treatment of both primary liver tumours as well as liver metastases might benefit from a triple combination inducing ferroptosis and supporting cytotoxic T cell function.

DISCUSSION

Cytotoxic CD8$^+$ T cells have the capacity to trigger tumour cell ferroptosis,[16] however, here we place ferroptosis upstream of immune cell activation and demonstrate that hepatocyte ferroptosis due to genetic *Gpx4* ablation causes a complex immune response including enhanced CD8$^+$ T cell recruitment as well as an immunosuppressive response that counteracts T cell activation. Induction of an adaptive T cell response in the context of cell death has led to the concept of immunogenic cell death.[34] However, generalisation of such concept has been questioned and several studies have shown that the inflammatory response to cell death does not necessarily lead to a strong adaptive immune response.[35 36] Our data challenge such generalisation further and highlight the complex balance between T cell activation and suppression that is even context dependent. Ferroptosis in the liver induced an antitumour response while simultaneously triggering two immunosuppressive pathways counterbalancing cytotoxic T cells. Ferroptotic hepatocytes released CXCL10, which in turn stimulated CD8$^+$ T cell infiltration into the tumour. CXCL10 release was dependent on the activation of the cGAS/STING pathway most likely due to 8-OHdG accumulation in *Gpx4*$^{Δ/Δhep}$ ferroptotic tumours as previously described for pancreatic cancer.[18] Ferroptosis did not only trigger CD8$^+$ T cell infiltration, but also induced IFNγ secretion by CD8$^+$ T cells, which caused enhanced PD-L1 expression on tumour cells. Moreover, by releasing HMGB1, ferroptosis induced MDSC infiltration in combination with PD-L1 upregulation shielded tumour cells from the ferroptosis-induced CD8 dependent antitumour activity. While histological analysis of livers suggested an increase of F4/80$^+$ TAMs, we could not validate this by flow cytometry. Therefore, the ferroptosis' effect on myeloid immunosuppressive cells seemed to be limited to MDSC whose immunosuppressive activity[37] was confirmed in an ex vivo T cell proliferation assay. Intriguingly, we could not find any significance difference in activation and exhaustion surface marker expression levels on CD8$^+$ T cells from Gpx4-deficient ferroptotic tumours or control tumours. It is surprising that T cells submitted to such a high immunosuppressive environment, with PD-L1 upregulation and MDSC activity, did not succumb to exhaustion, but on the contrary are more prone to secrete IFNγ. Further analysis will be required to understand CD8$^+$ T cell resistance to exhaustion in the context of ferroptosis.

This dichotomy and orchestrated response of inhibitory and activation signals has been extensively studied and well described for acute viral infection and T cell activation, where T cell activation is commonly associated with upregulation of inhibitory pathways to tune down T cell activation in the contraction phase

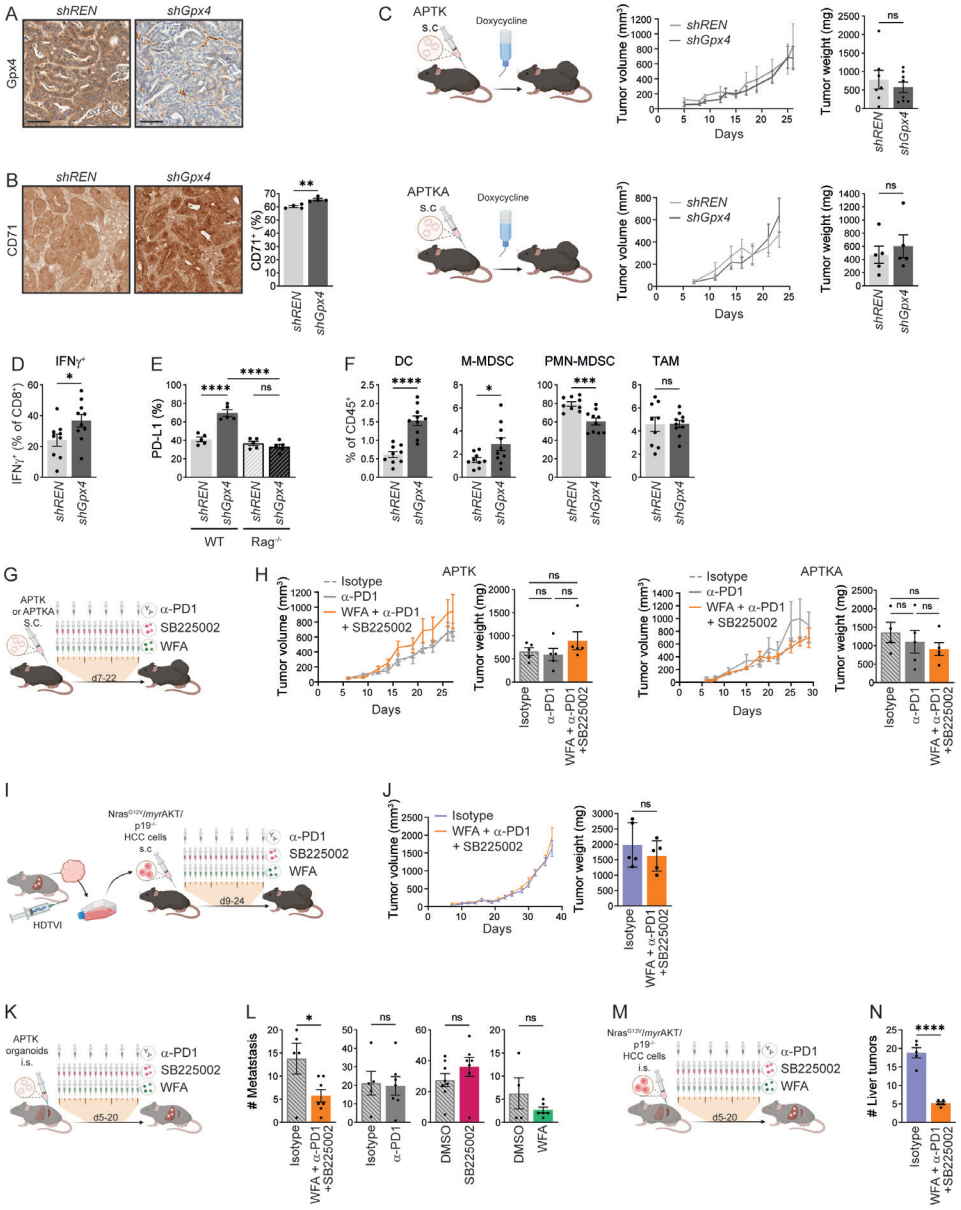

Figure 4 Ferroptosis effect on colorectal cancer. (A) Representative immunohistochemical Gpx4 staining of *shREN* or *shGPX4* APTKA s.c tumours. (B) Immunohistochemical quantification of $CD71^+$ cells in *shREN* and *shGpx4* APTKA s.c. tumours (n=4). (C) Tumour volumes and weights at end point of *shREN* and *shGpx4* APTK and ATPKA subcutaneous tumours (n≥5). (D) Flow cytometry analysis of IFNγ expression in $CD8^+$ T cells from *shREN* and *shGpx4* s.c. APTKA tumours, after ex vivo PMA/Ionomycin stimulation (n≥9). (E) Immunofluorescence quantification of PD-L1 expression in s.c *shREN* and *shGpx4* APTKA tumours from WT or $Rag^{-/-}$ mice (n=5). (F) Percentages of DC, M-MDSC, PMN-MDSC in immune infiltrates of *shREN* and *shGpx4* s.c. APTKA tumours analysed by flow cytometry (n≥9). (G) Treatment scheme after s.c. transplantation of APTK or APTKA organoids. (H) Tumour volumes and end point weights of s.c APTK and APTKA treated with the indicated compounds (n≥5). (I) Scheme for the isolation of $Nras^{G12V}$/*myr*AKT/$p19^{-/-}$ HCC cells followed by subcutaneous transplantation and treatments. (J) Tumour volumes and weights at end-point of subcutaneously transplanted $Nras^{G12V}$/*myr*AKT/$p19^{-/-}$ HCC cells with the indicated treatment. (K) Treatment scheme after intrasplenic (i.s.) injection of APTK organoids. (L) Numbers of liver metastasis after intrasplenic injection of APTK organoids and treatment as indicated (n≥4). (M) Treatment scheme after intrasplenic (i.s.) injection of $Nras^{G12V}$/*myr*AKT/$p19^{-/-}$ HCC cells. (N) Number of liver tumours after intrasplenic transplantation of $Nras^{G12V}$/*myr*AKT/$p19^{-/-}$ HCC cells and the indicated treatment (n≥5). (G, I, K, M) Scheme for i.p. injections, each represented by a syringe, with 250 µg of α-PD-1 or isotype (Rat IgG2a,κ), 2.5 mg/kg of Withaferin A (WFA) or 1 mg/kg of SB225002. (B–M) Data are mean±SEM, n.s not significant, *p≤0.05, ***p≤0.001, ****p≤0.0001 by t-test (B–F, J, L, N) one-way ANOVA with Šídák's multiple comparisons test (H) of the indicated pairs. ANOVA, analysis of variance; DC, dendritic cell; HCC, hepatocellular carcinoma; MDSC, myeloid derived suppressor cell; PMA, phorbol myristate acetate; s.c., subcutaneous.

and safeguard against 'self'-directed T cell activity. Therefore, in the context of immune-based cancer treatments a comprehensive analysis of the immune response needs to be implemented in order to identify potent anticancer agents whose antitumourigenic function would be masked by immunosuppressive activity that could be overcome by the right combinatorial treatment. We identified ferroptosis as such an example, where T cell activation is accompanied by PD-L1 and MDSC driven immunosuppression.

Importantly, T cell recruitment and consequent PD-L1 upregulation were observed in both models of primary HCC and colorectal cancer (CRC). However, while PD-1 blockade in HCC conferred a survival benefit, this was not the case in s.c. colorectal tumours. Also, the triple combination of WFA, SB225002 and α-PD-1 was only successful when liver tumours or metastases were treated, primary CRC did not respond to this approach. This suggests that the ferroptosis-induced immune response is not a general one but rather depends on the respective local microenvironment. Interestingly, in s.c. CRC we could not observe the pronounced PMN-MDSC accumulation we noticed in liver. Yet, this alone would not explain the unresponsiveness to checkpoint blockade of primary CRC tumours indicating that additional cellular mechanisms control immune response. Cancer-associated fibroblasts (CAFs) that are characterised by a high degree of heterogeneity may play an important role in this context as we have recently shown their potential to dictate the response to radiotherapy.[31] An important open question is the degree of interdependency between cancer cells, through their mutations, (neo)antigens, surface protein expression and secretome and the tumour environment. Our data demonstrate that the combination of inducing ferroptosis along with PD-1 and MDSC blockade does not rely on the presence of a particular tumour cell specific mutation and therefore such combination therapy could potentially be applied to any tumour type where the therapy's efficacy would be determined by the tumour microenvironment response to ferroptosis. Moreover, the individual components of a combination therapy could be adapted to the tumour environment with the ferroptosis inducing agent and α-PD-1 therapy as a basis. For management of liver cancers and CRC liver metastases, we illustrate that adding MDSC blockade is sufficient to establish a proper tumour suppression. For a direct clinical translation of our findings one should consider the caveat that we did not assess responsiveness of human HCC (different types or stages). Nevertheless, our data strongly suggest that the sensitivity of the primary tumour to this approach is irrelevant for the response of liver metastases of the same genetic background suggesting that such combinatorial treatment may be effective to treat liver metastases emerging from any cancer type.

Collectively, our data illustrate the complex interplay of tumour cell ferroptosis and adaptive immunity that provide the rationale for an innovative combinatorial treatment of primary liver tumours and metastases.

Author affiliations
[1]Institute for Tumor Biology and Experimental Therapy, Georg-Speyer-Haus, Frankfurt/Main, Germany
[2]Frankfurt Cancer Institute, Goethe University Frankfurt, Frankfurt/Main, Germany
[3]Department of Medicine I, Gastroenterology, Hepatology and Endocrinology, Goethe University Frankfurt, Frankfurt/Main, Germany
[4]University Medical Center Göttingen (UMG), Institute of Human Genetics, NGS-Integrative Genomics Core Unit (NIG), Göttingen, Germany
[5]Institute of Pathology, UniversitätsKlinikum Heidelberg, Heidelberg, Germany
[6]Center for Biomedical Science, The Feinstein Institute for Medical Research, Manhasset, New York, USA
[7]German Cancer Consortium (DKTK) and German Cancer Research Center (DKFZ), Heidelberg, Germany

Twitter Dominic Denk @DomDenkMD

Acknowledgements We thank Eva Rudolf, Preeti Gupta and Christin Danneil for expert technical assistance as well as the staff at the Animal Facility and the Histology and Flow Cytometry Core Facilities at the Georg-Speyer-Haus. We are grateful to Marcus Conrad for providing floxed Gpx4 mice as well as Daniel Dauch for providing murine liver tumour cell lines and thank Thomas Pleli for help with primary hepatocyte cultures. We thank the Else-Kröner-Fresenius-Stiftung (EKFS) for supporting his work.Graphical experimental schemes were created with BioRender.com.

Contributors CC, FF, DD, AN, KK, TWB, EE, YD and KM performed in vivo experiments and collected tissues samples. CC, FF, DD, KK, MP and TWB performed ex vivo experiments including the primary hepatocytes isolation and flow cytometry analysis. FF, CC, AN, FC and ÖC performed and analysed the IHC and IF staining. FF and ÖC performed qPCR experiments and analysis. GS performed RNAseq experiments. K-HP, SZ and TL provided support and expertise in the field of HCC. TL provided pathological assessment of liver histology. HY generated and provided the α-HMGB1 antibody for in vivo treatment. FRG conceptualised and supervised the study. CC, FF and FRG wrote the manuscript. FRG acts as guarantor.

Funding FF was supported by the 'Patenschaftsmodell' of the Goethe University Frankfurt and the Else-Kröner-Forschungskolleg. Work in the lab of FRG is supported by institutional funds from the Georg-Speyer-Haus, by the LOEWE Center Frankfurt Cancer Institute (FCI) funded by the Hessen State Ministry for Higher Education, Research and the Arts [III L 5 - 519/03/03.001 - (0015)], Deutsche Forschungsgemeinschaft (FOR2438: Gr1916/11-1; SFB1292-Project ID: 318346496-TP16; SFB1479-Project ID: 441891347-P02; GRK2336) and the ERC (Advanced Grant PLASTICAN-101021078). The Institute for Tumor Biology and Experimental Therapy, Georg-Speyer-Haus, is funded jointly by the German Federal Ministry of Health and the Ministry of Higher Education, Research and the Arts of the State of Hessen (HMWK).

Competing interests None declared.

Patient and public involvement Patients and/or the public were not involved in the design, or conduct, or reporting, or dissemination plans of this research.

Patient consent for publication Not applicable.

Provenance and peer review Not commissioned; externally peer reviewed.

Data availability statement Data are available on reasonable request. All data relevant to the study are included in the article or uploaded as online supplemental information.

ORCID iDs
Fabian Finkelmeier http://orcid.org/0000-0001-8559-9910
Kai-Henrik Peiffer http://orcid.org/0000-0002-3757-4476
Thomas Longerich http://orcid.org/0000-0001-8888-1030
Florian R Greten http://orcid.org/0000-0002-3928-6080

REFERENCES

1 Dixon SJ, Lemberg KM, Lamprecht MR, *et al*. Ferroptosis: an iron-dependent form of nonapoptotic cell death. *Cell* 2012;149:1060–72.
2 Fellmann C, Hoffmann T, Sridhar V, *et al*. An optimized microRNA backbone for effective single-copy RNAi. *Cell Rep* 2013;5:1704–13.
3 Chen X, Kang R, Kroemer G, *et al*. Ferroptosis in infection, inflammation, and immunity. *J Exp Med* 2021;218:e20210518.
4 Ursini F, Maiorino M, Valente M, *et al*. Purification from pig liver of a protein which protects liposomes and biomembranes from peroxidative degradation and exhibits glutathione peroxidase activity on phosphatidylcholine hydroperoxides. *Biochim Biophys Acta* 1982;710:197–211.

5 Friedmann Angeli JP, Krysko DV, Conrad M. Ferroptosis at the crossroads of cancer-acquired drug resistance and immune evasion. *Nat Rev Cancer* 2019;19:405–14.
6 Jiang L, Kon N, Li T, *et al*. Ferroptosis as a p53-mediated activity during tumour suppression. *Nature* 2015;520:57–62.
7 Zhang Y, Shi J, Liu X, *et al*. Bap1 links metabolic regulation of ferroptosis to tumour suppression. *Nat Cell Biol* 2018;20:1181–92.
8 Li J, Cao F, Yin H-L, *et al*. Ferroptosis: past, present and future. *Cell Death Dis* 2020;11:88.
9 Louandre C, Marcq I, Bouhlal H, *et al*. The retinoblastoma (Rb) protein regulates ferroptosis induced by sorafenib in human hepatocellular carcinoma cells. *Cancer Lett* 2015;356:971–7.
10 Ye Z, Liu W, Zhuo Q, *et al*. Ferroptosis: final destination for cancer? *Cell Prolif* 2020;53:e12761.
11 Hassannia B, Wiernicki B, Ingold I, *et al*. Nano-targeted induction of dual ferroptotic mechanisms eradicates high-risk neuroblastoma. *J Clin Invest* 2018;128:3341–55.
12 Mao L, Zhao T, Song Y, *et al*. The emerging role of ferroptosis in non-cancer liver diseases: hype or increasing hope? *Cell Death Dis* 2020;11:518.
13 Louandre C, Ezzoukhry Z, Godin C, *et al*. Iron-Dependent cell death of hepatocellular carcinoma cells exposed to sorafenib. *Int J Cancer* 2013;133:1732–42.
14 Jia M, Zhang H, Qin Q, *et al*. Ferroptosis as a new therapeutic opportunity for nonviral liver disease. *Eur J Pharmacol* 2021;908:174319.
15 Chen X, Kang R, Kroemer G, *et al*. Targeting ferroptosis in pancreatic cancer: a double-edged sword. *Trends Cancer* 2021;7:891–901.
16 Wang W, Green M, Choi JE, *et al*. $CD8^+$ T cells regulate tumour ferroptosis during cancer immunotherapy. *Nature* 2019;569:270–4.
17 Liao P, Wang W, Wang W, *et al*. $CD8^+$ T cells and fatty acids orchestrate tumor ferroptosis and immunity via ACSL4. *Cancer Cell* 2022;40:365–78.
18 Dai E, Han L, Liu J, *et al*. Ferroptotic damage promotes pancreatic tumorigenesis through a TMEM173/STING-dependent DNA sensor pathway. *Nat Commun* 2020;11:6339.
19 Dai E, Han L, Liu J, *et al*. Autophagy-Dependent ferroptosis drives tumor-associated macrophage polarization via release and uptake of oncogenic KRAS protein. *Autophagy* 2020;16:2069–83.
20 Efimova I, Catanzaro E, Van der Meeren L, *et al*. Vaccination with early ferroptotic cancer cells induces efficient antitumor immunity. *J Immunother Cancer* 2020;8:e001369.
21 Carlson CM, Frandsen JL, Kirchhof N, *et al*. Somatic integration of an oncogene-harboring sleeping Beauty transposon models liver tumor development in the mouse. *Proc Natl Acad Sci U S A* 2005;102:17059–64.
22 Canli Özge, Alankuş YB, Grootjans S, *et al*. Glutathione peroxidase 4 prevents necroptosis in mouse erythroid precursors. *Blood* 2016;127:139–48.
23 Carlson BA, Tobe R, Yefremova E, *et al*. Glutathione peroxidase 4 and vitamin E cooperatively prevent hepatocellular degeneration. *Redox Biol* 2016;9:22–31.
24 Feng H, Schorpp K, Jin J, *et al*. Transferrin receptor is a specific ferroptosis marker. *Cell Rep* 2020;30:3411–23.
25 Greten FR, Grivennikov SI. Inflammation and cancer: triggers, mechanisms, and consequences. *Immunity* 2019;51:27–41.
26 Rudalska R, Dauch D, Longerich T, *et al*. In vivo RNAi screening identifies a mechanism of sorafenib resistance in liver cancer. *Nat Med* 2014;20:1138–46.
27 Mowat C, Mosley SR, Namdar A, *et al*. Anti-Tumor immunity in mismatch repair-deficient colorectal cancers requires type I IFN-driven CCL5 and CXCL10. *J Exp Med* 2021;218:e20210108.
28 Li J, Sun J, Rong R, *et al*. Hmgb1 promotes myeloid-derived suppressor cells and renal cell carcinoma immune escape. *Oncotarget* 2017;8:63290–8.
29 Highfill SL, Cui Y, Giles AJ, *et al*. Disruption of CXCR2-mediated MDSC tumor trafficking enhances anti-PD1 efficacy. *Sci Transl Med* 2014;6:237ra67.
30 Varga J, Nicolas A, Petrocelli V, *et al*. Akt-Dependent Notch3 activation drives tumor progression in a model of mesenchymal colorectal cancer. *J Exp Med* 2020;217:e20191515.
31 Nicolas AM, Pesic M, Engel E, *et al*. Inflammatory fibroblasts mediate resistance to neoadjuvant therapy in rectal cancer. *Cancer Cell* 2022;40:168–84.
32 Seehawer M, Heinzmann F, D'Artista L, *et al*. Author correction: necroptosis microenvironment directs lineage commitment in liver cancer. *Nature* 2018;564:E9.
33 Soares KC, Foley K, Olino K, *et al*. A preclinical murine model of hepatic metastases. *J Vis Exp* 2014;51677:51677.
34 Galluzzi L, Buqué A, Kepp O, *et al*. Immunogenic cell death in cancer and infectious disease. *Nat Rev Immunol* 2017;17:97–111.
35 Ciampricotti M, Hau C-S, Doornebal CW, *et al*. Chemotherapy response of spontaneous mammary tumors is independent of the adaptive immune system. *Nat Med* 2012;18:344–6. author reply 6.
36 Hou J, Greten TF, Xia Q. Immunosuppressive cell death in cancer. *Nat Rev Immunol* 2017;17:401.
37 Bronte V, Brandau S, Chen S-H, *et al*. Recommendations for myeloid-derived suppressor cell Nomenclature and characterization standards. *Nat Commun* 2016;7:12150.